

Molecular dynamics simulations on the interactions between nucleic acids and a phospholipid bilayer

Yao Xu(徐耀), Shu-Wei Huang(黄舒伟), Hong-Ming Ding(丁泓铭), and Yu-Qiang Ma(马余强)

Citation: Chin. Phys. B, 2024, 33 (**2**): 028701. DOI: 10.1088/1674-1056/ad1178
Journal homepage: http://cpb.iphy.ac.cn; http://iopscience.iop.org/cpb

What follows is a list of articles you may be interested in

Resolution-enhanced single-pixel imaging using the Hadamard transform matrix

Shu-Hang Bie(别书航), Chen-Hui Wang(王晨晖), Rui-Bing Lv(吕瑞兵), Qian-Qian Bao(鲍倩倩),Qiang Fu(付强), Shao-Ying Meng(孟少英), and Xi-Hao Chen(陈希浩)

Chin. Phys. B, 2023, 32 (**12**): 128702. DOI: 10.1088/1674-1056/accf7d

Transverse manipulation of particles using Bessel beam of tunable size generated by cross-phase modulation

Xiang-Lai Qiao(乔响来), Xue-Mei Cheng(程雪梅), Qian Zhang(张倩), Wen-Ding Zhang(张文定), Zhao-Yu Ren(任兆玉), and Jin-Tao Bai(白晋涛)

Chin. Phys. B, 2023, 32 (**4**): 048703. DOI: 10.1088/1674-1056/ac8925

Effects of electric field on vibrational resonances in Hindmarsh-Rose neuronal systems for signal detection

Xiaoxia Li(李晓霞), Xiaopeng Xue(薛小鹏), Dongjie Liu(刘栋杰), Tianyi Yu(余天意), Qianqian He(何倩倩), and Guizhi Xu(徐桂芝)

Chin. Phys. B, 2023, 32 (**4**): 048701. DOI: 10.1088/1674-1056/ac9cc0

Investigations of moiré artifacts induced by flux fluctuations in x-ray dark-field imaging

Zhi-Li Wang(王志立), Zi-Han Chen(陈子涵), Yao Gu(顾瑶), Heng Chen(陈恒), and Xin Ge(葛昕)

Chin. Phys. B, 2023, 32 (**3**): 038704. DOI: 10.1088/1674-1056/ac946a

Analysis of refraction and scattering image artefacts in x-ray analyzer-based imaging

Li-Ming Zhao(赵立明), Tian-Xiang Wang(王天祥), Run-Kang Ma(马润康), Yao Gu(顾瑶), Meng-Si Luo(罗梦丝), Heng Chen(陈恒), Zhi-Li Wang(王志立), and Xin Ge(葛昕)

Chin. Phys. B, 2023, 32 (**2**): 028701. DOI: 10.1088/1674-1056/ac685d

---

Molecular dynamics simulations on the interactions between nucleic acids and a phospholipid bilayer

Yao Xu(徐耀)[1], Shu-Wei Huang(黄舒伟)[1], Hong-Ming Ding(丁泓铭)[2,†], and Yu-Qiang Ma(马余强)[1]

[1] *National Laboratory of Solid State Microstructures and Department of Physics, Collaborative Innovation Center of Advanced Microstructures, Nanjing University, Nanjing* 210093, *China*
[2] *Center for Soft Condensed Matter Physics and Interdisciplinary Research, School of Physical Science and Technology, Soochow University, Suzhou* 215006, *China*

(Received 2 October 2023; revised manuscript received 10 November 2023; accepted manuscript online 1 December 2023)

Recently, lipid nanoparticles (LNPs) have been extensively investigated as non-viral carriers of nucleic acid vaccines due to their high transport efficiency, safety, and straightforward production and scalability. However, the molecular mechanism underlying the interactions between nucleic acids and phospholipid bilayers within LNPs remains elusive. In this study, we employed the all-atom molecular dynamics simulation to investigate the interactions between single-stranded nucleic acids and a phospholipid bilayer. Our findings revealed that hydrophilic bases, specifically G in single-stranded RNA (ssRNA) and single-stranded DNA (ssDNA), displayed a higher propensity to form hydrogen bonds with phospholipid head groups. Notably, ssRNA exhibited stronger binding energy than ssDNA. Furthermore, divalent ions, particularly Ca^{2+}, facilitated the binding of ssRNA to phospholipids due to their higher binding energy and lower dissociation rate from phospholipids. Overall, our study provides valuable insights into the molecular mechanisms underlying nucleic acid-phospholipid interactions, with potential implications for the nucleic acids in biotherapies, particularly in the context of lipid carriers.

Keywords: RNA, DNA, lipid bilayer, molecular dynamics, interface interaction, divalent cation

PACS: 87.14.Cc, 87.14.G–, 87.15.ap, 87.16.D– **DOI:** 10.1088/1674-1056/ad1178

1. Introduction

Gene therapy has emerged as a novel therapeutic approach, addressing the genetic basis of diseases with promising potential.[1–4] Gene-based pharmaceutical formulations possess the capability to selectively express beneficial proteins and offer opportunities for vaccine applications and personalized medicine.[5] In this nucleic acid-based therapeutic strategy, genetic cargo is transported to target sites through specialized delivery systems, protecting against enzymatic degradation, immune reaction inhibition, and activation of efficient intracellular delivery mechanisms.[6–8] Consequently, current research efforts are focused on the development of non-viral vectors.[9–11] These vectors circumvent the associated drawbacks of viral vectors, such as the risks of genetic integration and increased immunogenicity.[12] However, the synthesis of such carriers currently faces challenges related to their relatively high levels of toxicity and low efficacy, necessitating the development of systems with optimized performance.[13] In this regard, lipid-based formulations have rapidly evolved as carriers in nucleic acid therapy due to their ability to accommodate long nucleic acid cargoes (e.g., mRNA or pDNA), low immunogenicity, and capacity for multiple dosing, enhancing therapeutic outcomes.[14,15] Formulations based on these lipid nanoparticles have already received approval from the United States Food and Drug Administration (FDA) and are poised to enter clinical development phases.[16]

Although previous and ongoing research endeavors have sought to rationally design ionizable lipid nanoparticles[17–23] for gene therapy applications, such as the self-assembly of polymeric single-chain RNA with ionizable cationic lipids,[24] which elucidated the timescale of self-assembly processes and the characteristics of the resulting complexes. Lipids with a cone-shaped geometry, such as DOPE, tend to facilitate the formation of the hexagonal II phase, thereby enhancing the endosomal release of antisense oligos.[25] However, the overall understanding of the physicochemical interactions governing the binding of zwitterionic lipids with single-chain nucleic acids remains limited, especially at the atomic level of their interactions. Molecular dynamics simulations, on the contrary, can offer valuable insights into their interactions from a microscopic view.[26–35] In this study, we aim to provide a detailed description of the interaction mechanisms involved in the binding process between single-chain nucleic acids and phospholipid bilayers, as well as the factors influencing these interactions through all-atom molecular dynamics simulations.

2. Model and methods

We first constructed ssRNA and ssDNA of various sequences using the online w3DNA[36] server (http://web.x3DNA.org/fibermodel/) (see Table 1). We then built the double-layer DOPC lipid membrane using the CHARMM-GUI server (https://charmm-gui.org).[37,38] Sub-

†Corresponding author. E-mail: dinghm@suda.edu.cn

© 2024 Chinese Physical Society and IOP Publishing Ltd

sequently, we performed separate 50 ns simulations for the single-stranded nucleic acids and the DOPC membrane in a 150 mM NaCl aqueous solution to achieve equilibrium, using GROMACS-2020.6[39,40] and the amber14sb_parmbsc1 force field.[41,42]

Next, we positioned the equilibrated single-stranded nucleic acids parallel to the principal axis of the equilibrated DOPC membrane at a distance of 3.5 nm from the center of the DOPC membrane (Fig. 1), employing Multiwfn[43] and VMD.[44] The initial box size was set to $6.5 \times 7.0 \times 12.5$ nm, and it was filled with approximately 12800 TIP3P water molecules. To maintain the electrical neutrality of the solution, a certain number of cations was added, and a 150 mM salt solution was included to simulate the physiological environment for nucleic acids. The system consisted of approximately 56000 atoms in total. The detailed simulated systems in this work are listed in Table 1.

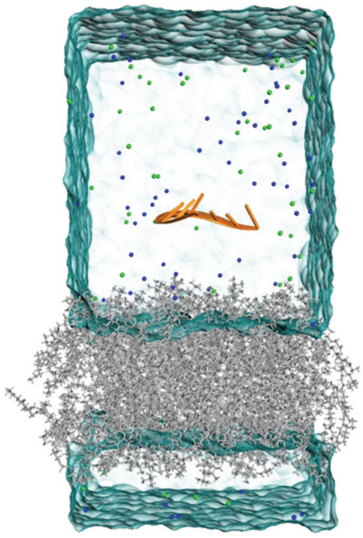


Fig. 1. Initial configuration of the MD simulations: the ssRNA (orange) engages with a DOPC membrane (gray), with Na^+ ions (blue) and Cl^- ions (green) regulating the environment. The water molecules are not shown for clarity.

The process of equilibrium simulation encompasses the following steps: initially, a total of 50000 steps of steepest descent energy minimization were performed, employing a maximum force constant of 1000 kJ/mol and employing the particle mesh Ewald (PME)[45] method to calculate the long-range electrostatic interactions. The Lennard–Jones interactions were computed using a truncation method with a cutoff radius of 1.0 nm. Subsequently, NVT (canonical ensemble) and NPT (isothermal-isobaric ensemble) pre-equilibrations were carried out over a duration of 10 ns. In the NVT ensemble, the V-rescale algorithm[46] was applied to scale velocities and maintain a constant temperature of 300 K. In the NPT ensemble, in addition to the aforementioned parameters, the Berendsen algorithm[47] and semi-isotropic coupling scheme were utilized to control pressure in the *xy*-plane and along the *z*-axis, with a target pressure set at 1 bar. Finally, the molecular dynamics (MD) simulation was conducted using a time step of 2 fs, and the Parrinello–Rahman algorithm[48] was employed for pressure coupling. Throughout the simulation, the structure, velocities, and energies of the system were saved every 100 ps, accumulating a total simulation time of 600 ns. For the MM-PBSA[49–52] calculations, the APBS[53] program was employed to solve the Poisson–Boltzmann equation, with a grid spacing of 0.045 nm, solute and solvent dielectric constants set to 2 and 78, respectively, a solvent-accessible surface probe radius of 0.14 nm, and a surface tension value of 0.027 kJ/(mol·Å^2).

Table 1. Simulated single-stranded nucleic acids-lipid bilayer systems.

System	Initial distance (nm)	Salt solution (150 mM)	Simulation time (ns)
ssRNA-A_{10}	3.5	NaCl	600
ssRNA-U_{10}	3.5	NaCl	600
ssRNA-C_{10}	3.5	NaCl	600
ssRNA-G_{10}	3.5	NaCl	600
ssRNA-A_8G_2	3.5	NaCl	600
ssRNA-A_6G_4	3.5	NaCl	600
ssRNA-A_4G_6	3.5	NaCl	600
ssRNA-A_2G_8	3.5	NaCl	600
ssDNA-A_{10}	3.5	NaCl	600
ssDNA-T_{10}	3.5	NaCl	600
ssDNA-C_{10}	3.5	NaCl	600
ssDNA-G_{10}	3.5	NaCl	600
ssRNA-A_{10}	3.5	KCl	600
ssRNA-A_{10}	3.5	$CaCl_2$	600
ssRNA-A_{10}	3.5	$MgCl_2$	600
ssDNA-A_{10}	3.5	KCl	600
ssDNA-A_{10}	3.5	$CaCl_2$	600
ssDNA-A_{10}	3.5	$MgCl_2$	600

3. Results and discussion

3.1. Interaction between ssRNA and the phospholipid bilayer

We first investigated the interaction of ssRNA with the lipid bilayer. As shown in Fig. 2, for the ssRNA-G_{10} system, we observed relatively stable adsorption of ssRNA to the lipid bilayer surface. In contrast, for the ssRNA-A_{10}, ssRNA-U_{10}, and ssRNA-C_{10} systems, the adsorption of RNA onto the lipid bilayer was unstable. This can be attributed primarily to the strong negative charge of the nucleic acid backbone and the electrostatic repulsion between the phosphate groups at the head of the lipid, making it generally difficult for ssRNA to approach the lipid bilayer. We then computed the distance between the ssRNA and the centroid of the lipid bilayer along the *z*-axis (Fig. 3(a)). It is found that, except for the ssRNA-G_{10} system, the distance fluctuated significantly over time in the other ssRNA systems. Actually, in the ssRNA-G_{10} system,

the ssRNA initially moves away from the phospholipid bilayer, which may be attributed to a significant electrostatic repulsion between the phosphate atoms of the nucleic acid backbone and the phosphate groups of the phospholipid bilayer. This repulsion is gradually weakened through a position adjustment process over approximately 50 ns, allowing the nucleic acid to approach the membrane. Notably, the thickness of the lipid monolayer is approximately 25 Å, while the distance in the ssRNA-G_{10} system stabilizes at around 23 Å, indicating that the ssRNA-G_{10} adsorbed on the surface of the phospholipid bilayer. We also calculated the contact surface area (CSA) between the ssRNA and the phospholipid bilayer over time. As shown in Fig. 3(b), for the ssRNA-G_{10} system, the CSA achieves stability within 200 ns and remains about 13 nm^2. In contrast, the other three single-chain RNA systems do not exhibit stable CSA within 600 ns.

The results indicate that the ssRNA-G_{10} is able to adsorb on the phospholipid bilayer firmly while the other three bases (A, C, U) are unable to form strong interactions for binding. Why there exist base-dependent adsorption behaviors? To answer this question, we first calculated the average number of hydrogen bonds between nucleic acid and phospholipid bilayer during the last 100 ns. As shown in Fig. 3(c), in the ssRNA-G_{10} system, 12.3 hydrogen bonds were observed during the last 100 ns, whereas in other base systems, the stable binding did not occur and hydrogen bonds were essentially absent. These results indicate a significant role of hydrogen bonds in the binding process of ssRNA to the phospholipid bilayer. In addition, we distinguished two types of hydrogen bonds, namely, those formed between the pentose sugars and the phospholipid, and those formed between the bases and the phospholipid. We found that the former only contributes to a small extent to ssRNA-lipid membrane interaction.

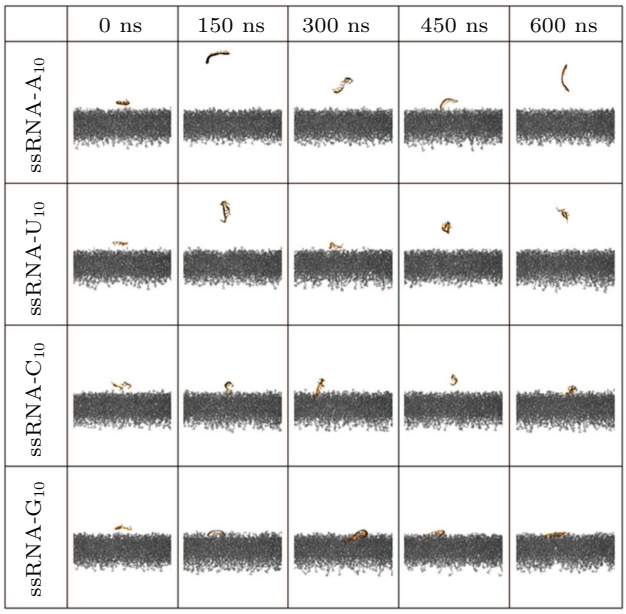


Fig. 2. Time-evolving snapshots illustrate the ssRNA and phospholipid system with four types of nucleobases. The nucleic acids and phospholipids are colored in orange and gray, respectively.

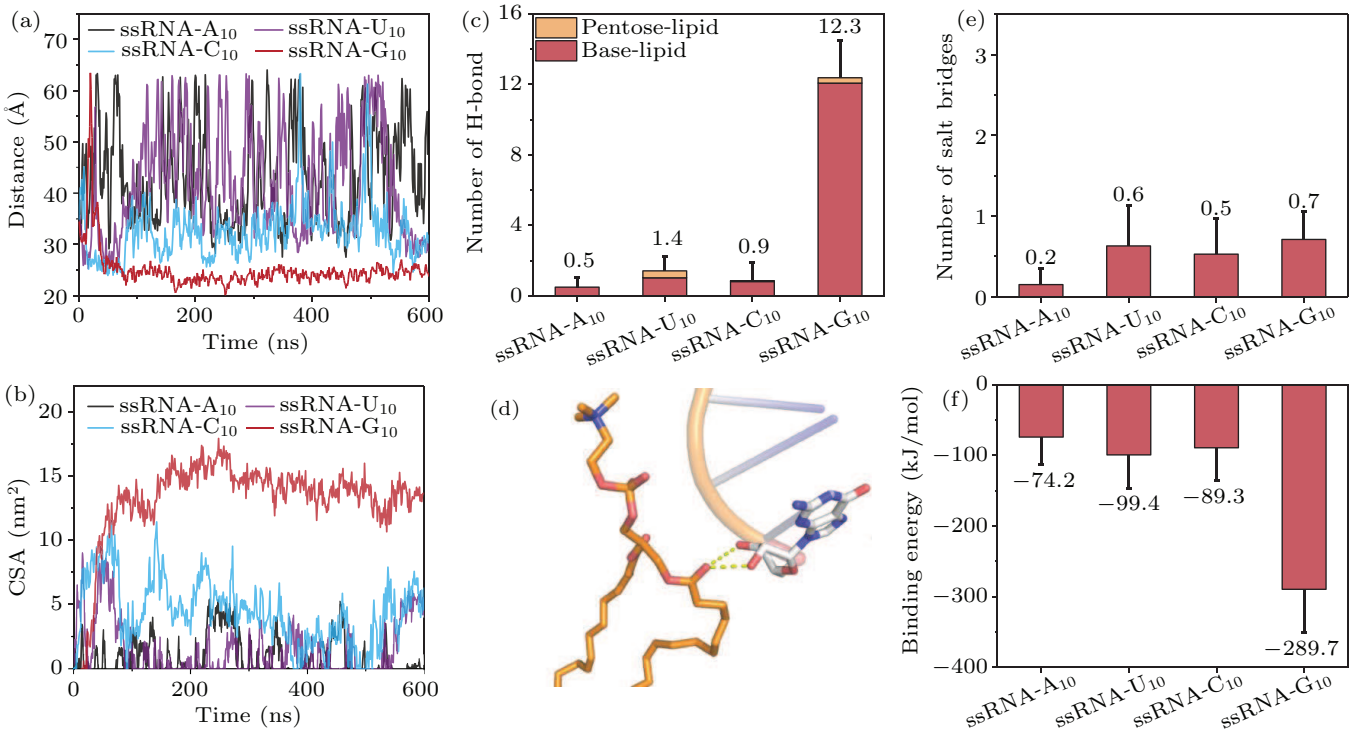


Fig. 3. Different types of nucleobases exhibit varying binding behaviors with the phospholipid bilayer. (a) The distance between the bilayer and ssRNA center of mass in the z-axis. (b) The contact surface area between the bilayer and ssRNA. (c) The number of hydrogen bonds formed between the bilayer and ssRNA's pentose and base in the last 100 ns. (d) The hydrogen bond between the pentose sugar of ssRNA and the carbonyl group in the middle of phospholipids. (e) The number of salt bridges between the bilayer and ssRNA in the last 100 ns. (f) Binding energy between the bilayer and ssRNA in the last 100 ns.

By examining the trajectories, we found that these hydrogen bonds mainly occur at the ends of ssRNA and only form hydrogen bonds with the carbonyl groups in the middle region of the phospholipid bilayer (Fig. 3(d)). This is because the position of the ribose sugar is close to the nucleic acid phosphate group. The negative charge of the nucleic acid phosphate group leads to significant repulsion with the phosphate groups at the head of the phospholipid bilayer. This results in a considerable distance between the nucleic acid ribose and the phospholipid bilayer headgroup, making the formation of this type of hydrogen bond difficult. As a result, most of the hydrogen bonds formed between nucleotides and the phospholipid bilayer involved nucleotides acting as hydrogen bond donors. This is attributed to the fact that the phospholipid bilayer headgroup primarily consists of carbon atoms with weaker electronegativity, which limits its ability to serve as a hydrogen bond donor to nucleic acids. Importantly, due to the highest number of hydrogen bond donors that guanine (G) possesses, it exhibits the greatest capacity for hydrogen bonding with the phospholipid. This characteristic of guanine's favorable hydrogen bonding with lipids compared to other bases has also been reported in a related study.[54]

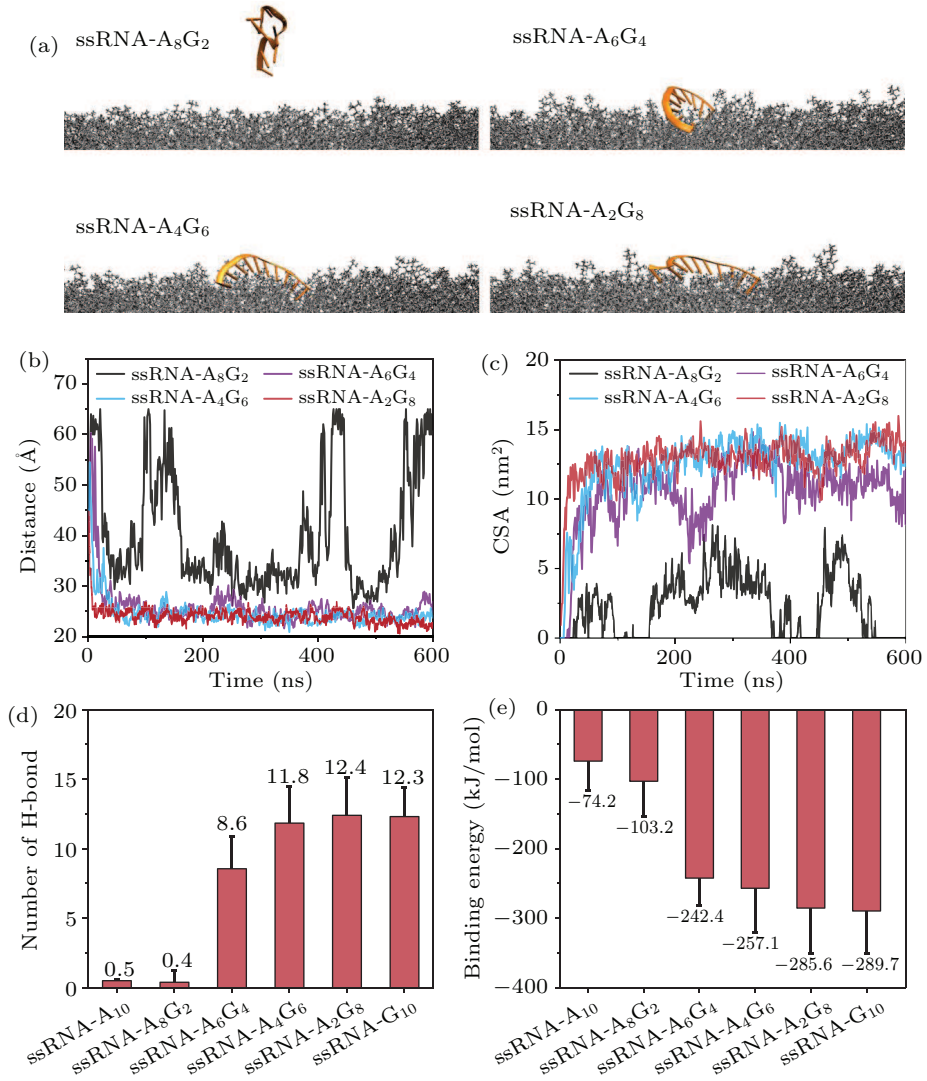


Fig. 4. The sequence of ssRNA can affect its binding to the bilayer. (a) Final snapshots depicting different sequences in each system. (b) Distance and (c) contact surface area between the bilayer and ssRNA. (d) The number of hydrogen bonds between the bilayer and ssRNA in the last 100 ns. (e) Binding energy between the bilayer and ssRNA in the last 100 ns.

Considering the presence of negatively charged phosphate groups on the ssRNA backbone and positively charged choline groups in the DOPC headgroup, salt bridges between ssRNA and the phospholipid bilayer are also plausible. However, as shown in Fig. 3(e), the number of salt bridges is small, and there is no apparent base selectivity, with relatively large error bars. Therefore, we can conclude that although salt bridges exist between ssRNA and the phospholipid bilayer during the stable binding process, hydrogen bonding still plays the dominant role and salt bridges merely contribute little. To characterize the adsorption preference of ssRNA to the phospholipid bilayer, we calculated the binding energy between ssRNA and the phospholipid bilayer via the MM-PBSA method. The energy values for each system are depicted in Fig. 3(f).

In the ssRNA-G_{10} system, with a higher number of hydrogen bonds, the binding energy is −289.7 kJ/mol, while in other systems with fewer hydrogen bonds, the binding energy remains below −100 kJ/mol, again indicating that ssRNA-G_{10} has the strongest affinity with the membrane.

Given the result that guanine can promote the binding between nucleic acid and the phospholipid bilayer through hydrogen bonding with the headgroup, we considered a series of sequence-mixed ssRNA to further validate this conjecture. Figure 4(a) illustrates the final snapshots of the mixed ssRNA interacting with the lipid membrane. By introducing guanine bases into the ssRNA-A_{10}, the binding between ssRNA and the phospholipid bilayer was gradually facilitated. As shown in Figs. 4(b) and 4(c), we observed that the ssRNA-A_8G_2 system, containing only two guanine bases, did not exhibit stable adsorption of nucleic acid to the phospholipid bilayer. Conversely, nucleic acid in the other three groups demonstrated stable adsorption to the phospholipid bilayer surface. In addition, the number of hydrogen bonds increased with an increasing number of guanine bases in the sequence, while the binding energy decreased (Figs. 4(d) and 4(e)). This indicates a progressively more stable binding between nucleic acid and the phospholipid bilayer. By increasing the ratio of guanine bases in the ssRNA sequence, the ssRNA is able to form more hydrogen bonds with the membrane, leading to an increased binding affinity.

3.2. Interaction between ssDNA and the phospholipid bilayer

We then explored the interaction between ssDNA and the phospholipid bilayer, and compared it with the ssRNA system. As shown in Fig. 5, we observed selective adsorption of ssDNA to the phospholipid bilayer, which is similar to that in the case of ssRNA. We then computed the centroid distance between ssDNA and the phospholipid bilayer in the z direction for various ssDNA systems. As shown in Fig. 6(a), consistent with the observations from the snapshots, only ssDNA-G_{10} exhibited stable binding to the phospholipid bilayer within 600 ns, while the other three bases did not demonstrate stable binding. However, we also observed that the stable distance of ssDNA-G_{10} from the phospholipid bilayer centroid was approximately 27 Å, slightly larger than the distance observed for ssRNA-G_{10} ($\sim$ 23 Å). Furthermore, in Fig. 6(b) the contact surface area between ssDNA-G_{10} and the lipid bilayer is about 8 nm^2, approximately 5 nm^2 smaller than that between ssRNA-G_{10} and the lipid bilayer ($\sim$ 13 nm^2). These findings indicate that the binding between ssRNA-G_{10} and the phospholipid bilayer is tighter than that between ssDNA-G_{10} and the phospholipid bilayer.

Generally, ssDNA adopts the B-form conformation with larger twist and rise, while ssRNA adopts the A-form conformation with smaller twist and rise. From the typical snapshots of both systems (Figs. 6(c) and 6(d)), we also observed significant differences in the stable binding modes of ssRNA-G_{10} and ssDNA-G_{10} to the phospholipid bilayer. ssRNA-G_{10} achieves stable binding by distorting its conformation, orienting all bases toward the phospholipid bilayer surface, thereby increasing the number of hydrogen bonds between nucleic acid and the membrane. On the other hand, ssDNA-G_{10} not only relies on hydrogen bonding between nucleic acid bases and the membrane but also stabilizes the binding by bringing the negatively charged nucleic acid phosphate groups close to the phospholipid bilayer surface (Fig. 6(c)), forming salt bridges with the positively charged choline groups at the head of the membrane. Notably, the flexibility of nucleic acid often plays an important role when it interacts with other molecules. To this end, we calculated the root-mean-square-fluctuation (RMSF) of ssRNA-G_{10} and ssDNA-G_{10}. As shown in Fig. S1, the ssRNA exhibits lower flexibility (more rigid) compared to ssDNA, which agrees with previous study.[55] Thus, the more flexible ssDNA may lose more degrees of freedom upon binding compared to ssRNA.

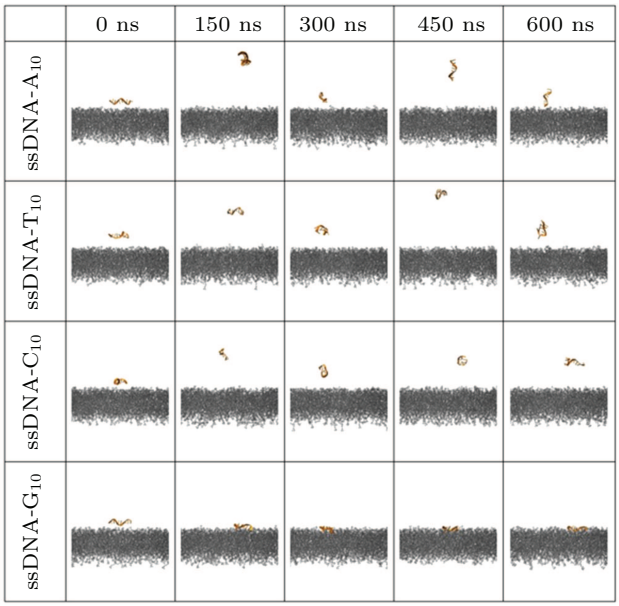


Fig. 5. Time-evolving snapshots illustrating the ssDNA and phospholipid system with four types of nucleobases. The nucleic acids and phospholipids are colored in orange and gray, respectively.

Furthermore, we also calculated the binding energies of ssDNA with the lipid membrane (Fig. 6(f)). The binding energy in ssDNA-G_{10} system (−189.1 kJ/mol) is much weaker than that in ssRNA-G_{10} system (−289.7 kJ/mol). This is because ssRNA-G_{10} exhibits a greater number of hydrogen bonds ($\sim$ 12.3) than ssDNA-G_{10} ($\sim$ 4.9). However, the binding energy in the ssDNA-A_{10} and ssDNA-C_{10} system is slightly stronger than that in the ssRNA-A_{10} and ssRNA-C_{10} system, which is probably because the number of salt bridges

in ssDNA systems is always greater than that in the corresponding ssRNA systems. In general, the interaction between ssRNA and the phospholipid bilayer is primarily hydrogen bond-driven, while the interaction between the ssDNA system and the phospholipid bilayer involves not only hydrogen bonding but also the participation of salt bridges.

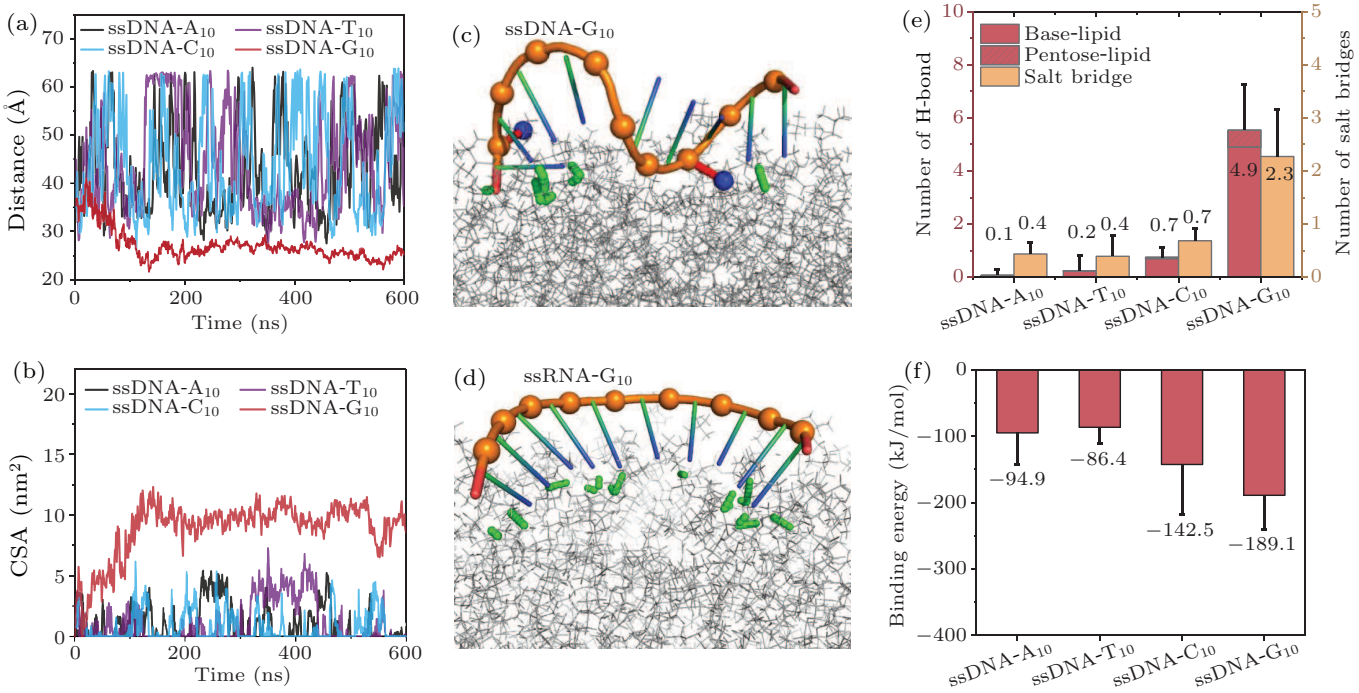


Fig. 6. In the case of ssDNA, different types of nucleobases also exhibit varying binding behaviors with the bilayer. (a) The distance between the bilayer and ssDNA center of mass in the z-axis. (b) The contact surface area between the bilayer and ssDNA. Snapshots of (c) ssDNA-G10 and (d) ssRNA-G10 binding with the phospholipid. Nitrogen atoms of the phospholipid choline are colored blue. The hydrogen bonds and salt bridges are represented with green and red dashed lines, respectively. (e) The number of hydrogen bonds and salt bridges between the bilayer and ssDNA in the last 100 ns. (f) Binding energy between the bilayer and ssDNA in the last 100 ns.

3.3. Effect of cation types on the interaction between single-stranded nucleic acids and the phospholipid bilayer

In our previous considerations, we focused on the presence of monovalent cations such as Na^+ (i.e., NaCl solution). In this section, we will examine the influence of other cations on the nucleic acid and the lipid bilayer. For the sake of simplicity, here we just take the ssRNA-A_{10} and ssDNA-A_{10} as an example. As shown in Fig. 7 and S2, it is observed that the addition of divalent cations such as Ca^{2+} or Mg^{2+} enables the stable binding of ssRNA-A_{10} and ssDNA-A_{10} to the phospholipid bilayer while K^+ and Na^+ cannot. Thus, compared to monovalent cations, divalent cations are more effective in promoting the binding between ssRNA/ssDNA and the phospholipid bilayer. Figures 8(a) and 8(b) present the centroid distance between the nucleic acid and the phospholipid bilayer in the z-direction. It can be observed that all divalent cations can significantly enhance the binding of both ssRNA and ssDNA to the bilayer. However, after stable binding, the binding distance of ssRNA-A_{10} (around 22 Å) is significantly smaller than ssDNA-A_{10} (around 32 Å). As shown in Figs. 8(c) and 8(d), the contact surface area of ssDNA and ssRNA with the bilayer is also different, where ssDNA-A_{10} (around 5 nm^2) has a smaller contact area compared to ssRNA-A_{10} (around 8 nm^2). The underlying reason for the variation in binding to the bilayer between ssRNA-A_{10} and ssDNA-A_{10} is akin to the earlier conclusion, stemming from the structural flexibility and subtle distinctions in secondary structure. The A-form configuration of ssRNA enables more extensive interactions with the phospholipid bilayer, leading to a firmer binding to the bilayer.

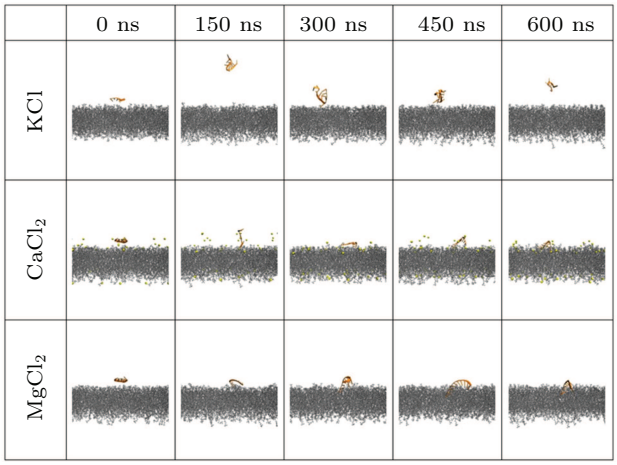


Fig. 7. Time-evolving snapshots of ssRNA-A10 and the bilayer with different ions (K^+, Ca^{2+}, Mg^{2+}).

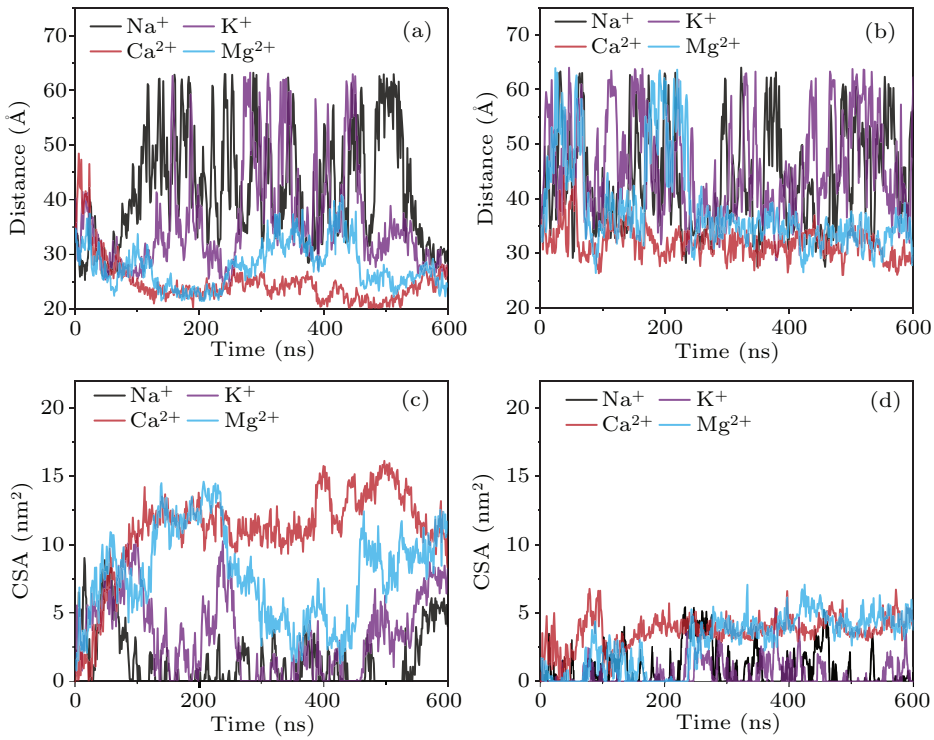


Fig. 8. The z-axis distance between the bilayer and (a) ssRNA and (b) ssDNA. The contact surface area between the bilayer and (c) ssRNA and (d) ssDNA.

We then studied the distinct role of cations in the binding of ssRNA-A_{10} to phospholipid bilayers. Generally, the propensity of Ca^{2+} to induce adsorption stems from its robust adherence to the phospholipid bilayer, resulting in a positively charged surface. Consequently, negatively charged nucleic acids are capable of approaching the phospholipid bilayer and establishing stable associations through the formation of salt bridges and hydrogen bonds. By quantifying the numbers of Ca^{2+} on the phospholipid bilayer surface, as depicted in Fig. 9(a), we ascertain a pronounced tendency of Ca^{2+} ions to adsorb onto the membrane. There are approximately 45 Ca^{2+} ions adsorbed on the phospholipid bilayer surface, while the overall number of Ca^{2+} ions in the entire system is merely 57. The adsorption of divalent cations leads to a positively charged surface on the phospholipid bilayer. Due to the strong negative charge of the nucleic acid phosphate groups, electrostatic forces draw the nucleic acid towards the phospholipid bilayer. Simultaneously, this phenomenon could potentially lead to the binding of phosphate groups on the nucleic acid to either the Ca^{2+} ions on the phospholipid bilayer surface or the positively charged choline groups on the lipid headgroups. Therefore, we further computed the number of contacts between the phosphate groups of the nucleic acid and the choline groups of the phospholipid bilayer (Prna-Npc) as well as the contacts between the bridged phosphate groups of the membrane and the nucleic acid facilitated by Ca^{2+} ions (referred to as Ppc-Ca-Prna in Fig. 9(a)).

Given the strong adsorption of Ca^{2+} on the phospholipid bilayer surface, as observed in Fig. 9(a), we anticipate a similar phenomenon for Mg^{2+}, which is also a divalent ion. However, as shown in Fig. 9(b), Mg^{2+} does not exhibit similar adsorption on the phospholipid bilayer surface as Ca^{2+}, but rather follows a distribution pattern similar to that of monovalent ions such as K^+ and Na^+, appearing to be uniformly distributed in the aqueous solution. The reason for difference in density distributions may be due to their different charge densities. Mg^{2+} has a higher charge density due to smaller size, which makes its hydration shell more stable, while Ca^{2+} is more likely to lose its outer water shell, allowing it to better interact with the bilayer.[56] This finding confirms our earlier hypothesis that Mg^{2+} and Ca^{2+} possess different mechanisms in promoting the binding of nucleic acids to phospholipid bilayers. The phenomenon of stronger adsorption of Ca^{2+} on the phospholipid bilayer compared to other ions has been previously reported in the literature.[57–59] These studies indicate that the efficiency of these ions in binding to phospholipid bilayers follows the order: $Ca^{2+} > Mg^{2+} > Na^+ > K^+$.

We next analyzed the influence of different ions on the nucleic acids. Based on the root-mean-square deviation (RMSD) analysis (Fig. 9(c)), it is evident that Ca^{2+} exerts the most pronounced influence on the structure of ssRNA. Figure 9(d) shows the presence of approximately 3 to 6 divalent ions surrounding the nucleic acid. Since the nucleic acid backbone carries a negative charge of $-9e$, divalent ions can effectively

screen the negative charge of the nucleic acid backbone. In contrast, the number of monovalent ions surrounding the nucleic acid is small, typically one or two, which is insufficient to shield the negative charge of the nucleic acid backbone, resulting in significant electrostatic repulsion between the nucleic acid and the zwitterionic phospholipid bilayer. Moreover, by comparing the number of divalent ions surrounding the nucleic acid, we observe that the number of Ca^{2+} ions around the nucleic acid is slightly higher than Mg^{2+}, approximately 1 to 2 more. Moreover, from the fluctuation of their respective curves, it is evident that Ca^{2+} ions exhibit a more stable presence around the nucleic acid. This suggests the formation of more stable salt bridges between Ca^{2+} and the nucleic acid, enabling better shielding of the negative charge of the nucleic acid backbone.

We further calculated the average number of hydrogen bonds and salt bridges in different systems (Figs. 9(e) and 9(f)). For the monovalent-cation system, the numbers of hydrogen bonds and salt bridges are both small, which cannot generate the adsorption of ssRNA to the lipid bilayer. While for the divalent-cation system, the Mg^{2+} system exhibits a similar pattern as the Ca^{2+} system, where both salt bridges and hydrogen bonds contribute to the stable binding of nucleic acids and phospholipid bilayers (Fig. 10). However, compared to the Ca^{2+} system, the Mg^{2+} system has fewer salt bridges and hydrogen bonds, thereby having a weaker affinity for the phospholipid bilayer surface.

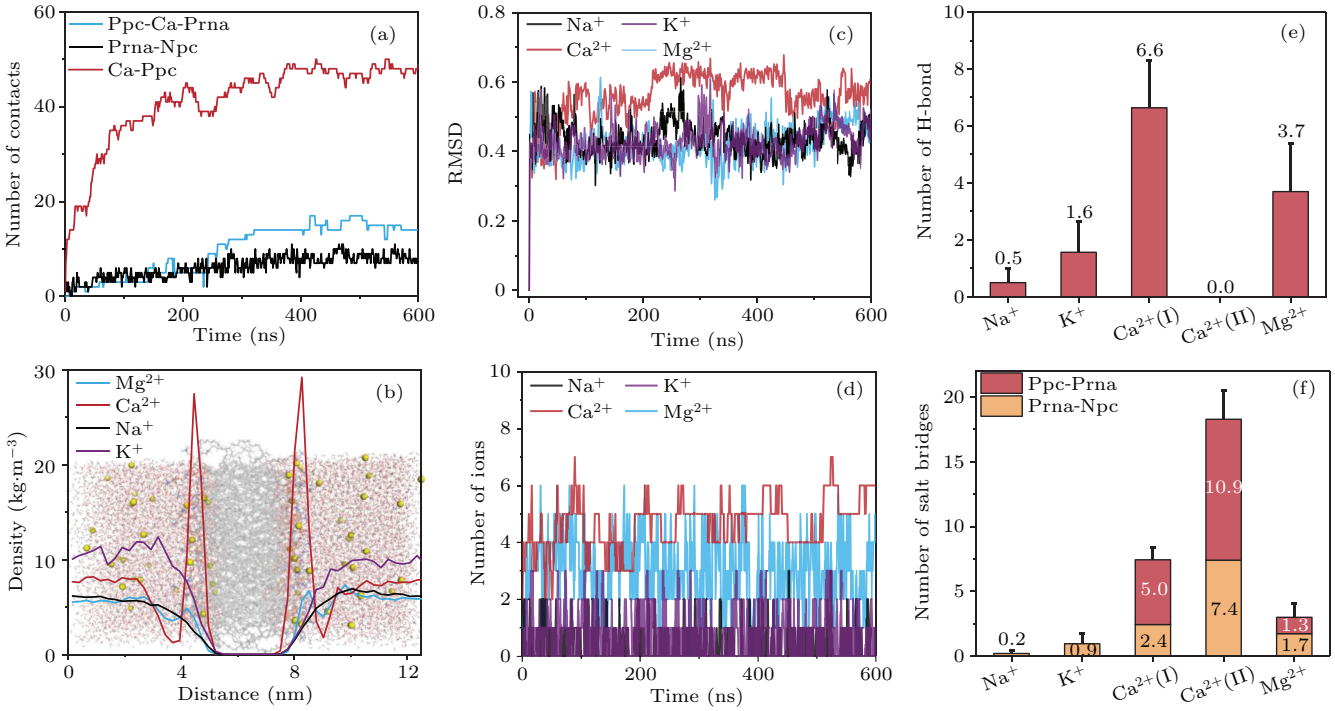


Fig. 9. (a) The number of salt bridges mediated by Ca^{2+} (blue) and the contact number of Prna-Npc (black) and Ca^{2+}-Ppc (red). (b) The density distribution of ions along the z-axis in the last 100 ns. (c) RMSD of ssRNA in different systems. (d) Numbers of ions around ssRNA during the simulations. The number of (e) hydrogen bonds and (f) salt bridges between ssRNA and bilayer within the last 100 ns.

Interestingly, we also discovered another mode (referred to as Ca^{2+}(II)) by which Ca^{2+} facilitates the adsorption of nucleic acids to the phospholipid bilayer. This mode lacks hydrogen bonds and relies solely on two types of salt bridges in Fig. 9(f) (Ppc-Ca-Prna and Prna-Npc). To maintain stable interactions between nucleic acids and the phospholipid bilayer, the total number of salt bridges in this mode can reach as high as 18.3. The rationale behind this mode can be inferred from the snapshot, namely, due to the curved structure of nucleic acids, when the predominantly negatively charged phosphate groups of the nucleic acid backbone are tightly bound to the phospholipid surface by Ca^{2+}, the nucleic acid bases face away from the phospholipid surface, rendering hydrogen bond formation with the phospholipid surface impossible. As the adsorption becomes more stable, the likelihood of hydrogen bond formation diminishes, leading to the formation of the Ca^{2+}(II) mode.

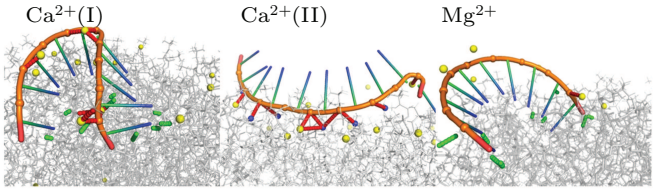


Fig. 10. Illustration of ions-mediated ssRNA and bilayer binding. Nitrogen atoms of the phospholipid choline and ions are shown in blue and yellow spheres. The hydrogen bonds and salt bridges are represented with green and red dashed lines.

4. Conclusions

In summary, we conducted all-atom molecular dynamics simulations to investigate the interactions between single-stranded nucleic acids and phospholipids. We observed selective adsorption of ssRNA to phospholipids, with greater hydrophilic bases exhibiting a higher propensity for hydrogen bonding with phospholipids. Specifically, increasing the presence of base G in the hybrid sequence enhanced the adsorption between nucleic acids and phospholipids. Furthermore, we identified differences in the interactions between ssDNA and ssRNA with phospholipids due to their structural disparities. In the ssDNA system, both hydrogen bonds and the Pdna-Npc salt bridge played dominant roles, while in the ssRNA system, hydrogen bonding alone was the primary driving force. Additionally, we investigated the impact of different ions on the interaction between ssRNA and phospholipids. We found that divalent ions, such as Ca^{2+} and Mg^{2+}, effectively facilitated the binding of ssRNA to phospholipids by shielding the negative charges of the nucleic acid backbone. However, the mechanisms by which Ca^{2+} and Mg^{2+} promoted the interaction differed. Ca^{2+} not only shielded the negative charges of the nucleic acid but also strongly adsorbed to the phospholipid surface, resulting in its positive charge and the formation of bridges between nucleic acid phosphate groups and phospholipid phosphate groups. While Ca^{2+} demonstrated superior ability to promote the adsorption of nucleic acids on DOPC membranes, it is worth noting that, compared to Ca^{2+}, Mg^{2+} plays an important role in stabilizing the structure of nucleic acids. Therefore, when conducting research related to nucleic acids-lipid bilayer interaction, it is crucial to handle the choice of ions with consideration. In summary, this study elucidated the molecular-level interactions between single-stranded nucleic acids and phospholipid bilayers, providing insights for the development of more stable and efficient lipid carriers in the experiments.

Acknowledgements

Project supported by the National Natural Science Foundation of China (Grant Nos. 12222506, 12347102, and 12174184). We are grateful to the High Performance Computing Center (HPCC) of Nanjing University for performing the numerical calculations in this paper on its blade cluster system.

References

[1] Sung Y K and Kim S W 2019 *Biomater. Res.* **23** 8
[2] Anguela X M and High K A 2019 *Annu. Rev. Med.* **70** 273
[3] Angell C, Xie S, Zhang L and Chen Y 2016 *Small* **12** 1117
[4] Guan S and Rosenecker J 2017 *Gene. Ther.* **24** 133
[5] Hajj K A and Whitehead K A 2017 *Nat. Rev. Mater.* **2** 17056
[6] Lostalé-Seijo I and Montenegro J 2018 *Nat. Rev. Chem.* **2** 258
[7] Mo F, Jiang K, Zhao D, Wang Y, Song J and Tan W 2021 *Adv. Drug. Deliv. Rev.* **168** 79
[8] Hu Q, Li H, Wang L, Gu H and Fan C 2018 *Chem. Rev.* **119** 6459
[9] Guan S and Rosenecker J 2017 *Gene. Ther.* **24** 133
[10] Kanasty R, Dorkin J R, Vegas A and Anderson D 2013 *Nat. Mater.* **12** 967
[11] Yin H, Kanasty R L, Eltoukhy A A, Vegas A J, Dorkin J R and Anderson D G 2014 *Nat. Rev. Genet.* **15** 541
[12] Thomas C E, Ehrhardt A and Kay M A 2003 *Nat. Rev. Genet.* **4** 346
[13] Vega-Villa K R, Takemoto J K, Yáñez J A, Remsberg C M, Forrest M L and Davies N M 2008 *Adv. Drug. Deliv. Rev.* **60** 929
[14] Fenton O S, Kauffman K J, McClellan R L, Appel E A, Dorkin J R, Tibbitt M W, Heartlein M W, De Rosa F, Langer R and Anderson D G 2016 *Adv. Mater.* **28** 2939
[15] Geall A J, Verma A, Otten G R, Shaw C A, Hekele A, Banerjee K, Cu Y, Beard C W, Brito L A, Krucker T, O'Hagan D T, Singh M, Mason P W, Valiante N M, Dormitzer P R, Barnett S W, Rappuoli R, Ulmer J B and Mandl C W 2012 *Proc. Natl. Acad. Sci. USA* **109** 14604
[16] Thess A, Grund S, Mui B L, Hope M J, Baumhof P, Fotin-Mleczek M and Schlake T 2015 *Mol. Ther.* **23** 1456
[17] Fenton O S, Kauffman K J, Kaczmarek J C, McClellan R L, Jhunjhunwala S, Tibbitt M W, Zeng M D, Appel E A, Dorkin J R, Mir F F, Yang J H, Oberli M A, Heartlein M W, DeRosa F, Langer R and Anderson D G 2017 *Adv. Mater.* **29** 201606944
[18] Samaridou E, Heyes J and Lutwyche P 2020 *Adv. Drug. Deliv. Rev.* **154–155** 37
[19] Semple S C, Klimuk S K, Harasym T O, Dos Santos N, Ansell S M, Wong K F, Maurer N, Stark H, Cullis P R, Hope M J and Scherrer P 2001 *Biochim. Biophys. Acta Biomembr.* **1510** 152
[20] Tam P, Monck M, Lee D, Ludkovski O, Leng E C, Clow K, Stark H, Scherrer P, Graham R W and Cullis P R 2000 *Gene. Ther.* **7** 1867
[21] Heyes J, Palmer L, Chan K, Giesbrecht C, Jeffs L and MacLachlan I 2007 *Mol. Ther.* **15** 713
[22] Hou X, Zaks T, Langer R and Dong Y 2021 *Nat. Rev. Mater.* **6** 1078
[23] Czerniak T and Saenz J P 2022 *Proc. Natl. Acad. Sci. USA* **119** e2119235119
[24] Rissanou A N, Ouranidis A and Karatasos K 2020 *Soft Matter* **16** 6993
[25] Cheng X and Lee R J 2016 *Adv. Drug. Deliv. Rev.* **99** 129
[26] Arnott P M, Joshi H, Aksimentiev A and Howorka S 2018 *Langmuir* **34** 15084
[27] Schlich M, Palomba R, Costabile G, Mizrahy S, Pannuzzo M, Peer D and Decuzzi P 2021 *Bioeng. Transl. Med.* **6** e10213
[28] Ding H, Li J, Chen N, Hu X, Yang X, Guo L, Li Q, Zuo X, Wang L, Ma Y and Fan C 2018 *ACS Cent. Sci.* **4** 1344
[29] Qiang X W, Zhang C, Dong H L, Tian F J, Fu H, Yang Y J, Dai L, Zhang X H and Tan Z J 2022 *Phys. Rev. Lett.* **128** 108103
[30] Xu Y, Huang S W, Ma Y Q and Ding H M 2022 *Nanoscale. Adv.* **4** 754
[31] Chen P, Yue H, Zhai X, Huang Z, Ma G H, Wei W and Yan L T 2019 *Sci. Adv.* **5** eaaw319
[32] Li X, Zhou S and Lin X 2022 *J. Chem. Inf. Model* **62** 2421
[33] Zou A, Lee S, Li J and Zhou R 2020 *J. Phys. Chem. B* **124** 701
[34] Chen X, Tian F, Li M, Xu H, Cai M, Li Q, Zuo X, Wang H, Shi X, Fan C, Baigude H and Shan Y 2020 *Global Chal.* **4** 1900075
[35] Liu Q, Wang H, Shi X, Wang Z G and Ding B 2017 *ACS Nano* **11** 7251
[36] Lu X J and Olson W K 2003 *Nucleic. Acids. Res.* **31** 5108
[37] Wu E L, Cheng X, Jo S, Rui H, Song K C, Dávila-Contreras E M, Qi Y, Lee J, Monje-Galvan V, Venable R M, Klauda J B and Im W 2014 *J. Comput. Chem.* **35** 1997
[38] Park S, Choi Y K, Kim S, Lee J and Im W 2021 *J. Chem. Inf. Model.* **61** 5192
[39] Abraham M J, Murtola T, Schulz R, Páll S, Smith J C, Hess B and Lindah E 2015 *SoftwareX* **1–2** 19
[40] Berendsen H J C, van der Spoel D and van Drunen R 1995 *Comput. Phys. Commun.* **91** 43
[41] Maier J A, Martinez C, Kasavajhala K, Wickstrom L, Hauser K E and Simmerling C 2015 *J. Chem. Theory. Comput.* **11** 3696
[42] Ivani I, Dans P D, Noy A, Pérez A, Faustino I, Hospital A, Walther J, Andrio P, Goñi R, Balaceanu A, Portella G, Battistini F, Gelpí J L, González C, Vendruscolo M, Laughton C A, Harris S A, Case D A and Orozco M 2015 *Nat. Methods* **13** 55
[43] Lu T and Chen F 2012 *J. Comput. Chem.* **33** 580
[44] Humphrey W, Dalke A and Schulten K 1996 *J. Mol. Graph.* **14** 33

[45] Essmann U, Perera L, Berkowitz M L, Darden T, Lee H and Pedersen L G 1995 *J. Chem. Phys.* **103** 8577
[46] Bussi G, Donadio D and Parrinello M 2007 *J. Chem. Phys.* **126** 014101
[47] Berendsen H J C, Postma J P M, Van Gunsteren W F, Dinola A and Haak J R 1984 *J. Chem. Phys.* **81** 3684
[48] Parrinello M and Rahman A 1981 *J. Appl. Phys.* **52** 7182
[49] Wang C, Greene D, Xiao L, Qi R and Luo R 2018 *Front Mol. Biosci.* **4** 87
[50] Ding H M, Yin Y W, Ni S D, Sheng Y J and Ma Y Q 2021 *Chin. Phys. Lett.* **38** 18701
[51] Chen Y Q, Sheng Y J, Ding H M and Ma Y Q 2022 *Chin. Phys. B* **31** 048701
[52] Yan Z S, Xu Y, Ding H M and Ma Y Q 2022 *Chin. Phys. Lett.* **39** 108701
[53] Baker N A, Sept D, Joseph S, Holst M J and McCammon J A 2001 *Proc. Natl. Acad. Sci. USA* **98** 10037
[54] Elder R M and Jayaraman A 2013 *Soft Matter* **9** 11521
[55] Chen H, Meisburger S P, Pabit S A, Sutton J L, Webb W W and Pollack L 2012 *Proc. Natl. Acad. Sci. USA* **109** 799
[56] Barger J P and Dillon P F 2020 *Electrophoresis* **41** 1170
[57] Mao Y, Du Y, Cang X, Wang J, Chen Z, Yang H and Jiang H 2013 *J. Phys. Chem. B* **117** 850
[58] Abhinav, Jurkiewicz P, Hof M, Allolio C and Sykora J 2022 *Biomolecules* **12** 1894
[59] Tao Z, Yunguang Q, Qichao L, Xi C, Lifen Z, Xin Y, Bo P, Hualiang J and Huaiyu Y 2019 *Acta Physico-Chimica Sinica* **35** 840